Supplementary Materials for

High Density Assembling of Energetic Molecules under Constrain of Defected 2D Materials

Qi-Long Yan*[1], Zhijian Yang[2], Xue-Xue Zhang[1], Jie-Yao Lyu[1], Wei He[1], Shi Huang[2], Pei-Jin Liu[1], Chaoyang Zhang[2], Qing-Hua Zhang[2], Guo-Qiang He[1], Fu-De Nie[2]

1. Science and Technology on Combustion, Internal Flow and Thermo-structure Laboratory, Northwestern Polytechnical University, Xi'an 710072, China; 2. Institute of Chemical Materials, CAEP, Mianyang, 621900, China.

S1. Experimental

S1.1 Materials

HMX and RDX were commercially available without further purification (purity > 99.5%). TAG•HNO_3 were synthesized and purified after an optimized recrystallization before its usage in this research. The analytical pure glyoxal solution (37 vol.%), DMSO, acetone, ethyl acetate and deionized water used in the present study were commercially available and used as they were without further purification.

S1.2 Preparation of Nitramine/TAGP hybrid crystals

As an example, the preparation procedure for HT-0 can be described as follows: 0.60 g TAG•HNO_3 (TAGN) was dissolved in 20 mL DMSO completely with constant stirring at 70 ˚C. After that, 2.23 g HMX was added to the solution with stirring for 30 min. The mole ratio of HMX to TAGN is 1:2. Keeping the mixture in a water bath with controlled temperature of 70 ℃, and then 0.72 g glyoxal solution was added to the mixture, stirring for 1 h. In this step, the 2D polymer TAGP was *in-situ* synthesized from TAGN and glyoxal *via* condensation polymerization (see in Fig.1A). A certain amount of deionized water was added dropwise, and light grey crystals (see in fig. S1) could be gradually precipitated. Finally, the crystals were filtered and dried under vacuum. The synthetic procedures of HT-1, HT-2, HT-3, HT-4, HT-5, and HT-7 are very similar to that of HT-0. As the comparative parallel experiments, the mole ratios of TAGN to glyoxal for HT-1, HT-2, HT-3, HT-4, HT-5, and HT-7 were set to be 1:3, 1:7, 1:7, 1:7, 1:7, and 1:3 under reaction temperature of 70, 70, 150, 100, 120, and 150 ˚C, respectively. The experimental conditions and the uses of the raw materials are listed in Table S0.

Table S0. The experimental conditions and starting materials for the target products

Sample(mole ratio)	TAGN (g)	DMSO (ml)	HMX (g)	Glyoxal (g)	*T* (˚C)
HT-0(1:2)	0.60	20	2.23	0.72	70
HT-1(1:3)	0.48	15	2.96	0.54	70
HT-2(1:7)	0.24	15	2.66	0.27	70
HT-3(1:7)	0.24	15	2.66	0.27	150
HT-4(1:7)	0.24	15	2.66	0.27	100
HT-5(1:7)	0.24	15	2.66	0.27	120
HT-7(1:3)	0.51	15	2.66	0.62	150

Moreover, the preparation procedure of HT-6 (modified HMX crystal for single crystal X-ray diffraction) is as follows: the HT-4 (it is equivalent to use HT-1 or HT-7) was dissolved in acetone/ethyl acetate with 1/1 volume ratio in with magnetic stirring for 30 min. Then the pure crystals were separated with the doping TAGP layered material after vaporization of the solvents slowly under ambient condition for 48 h. We could observe the partially dispersed of the conjugated polymer TAGP with the aggregation/stacking, and meantime HMX molecules with modified conformation crystallized separately. In the end, the crystals were picked out and dried under ambient conditions for X-ray measurement. The modified RDX crystal for single crystal X-Ray diffraction measurement was prepared at the same conditions that were used to prepare HT-4, and the following method to prepare HT-6.

S1.3 Characterization and performances

Structures and morphologies: The morphologies of the specimens were recorded by using a scanning electron microscope (SEM; JSM-6390LV, Zeiss). The surface chemistry was analyzed using X-ray photoelectron spectroscopy (XPS; ThermoFisher spectrometer) equipped with monochromatic Al Kα radiation (1486.6 eV). All measurements were done in hybrid mode, at a 90° take off angle and a spot size of 400 μm. Elemental core-level spectra were fit using Avantage software (ThermoFisher). The binding energy of the spectra was calibrated with respect to C 1s peak (C–C(H), 284.6 eV). After subtraction of a Shirley background, all spectra were fit with the use of a convolution of Lorentzian and Gaussian shapes at a standard ratio of 30:70. Raman measurements were performed with an FT-Raman spectrometer (DXR SmartRaman). The excitation source was 532 nm from surface plasmon resonance. To avoid the photochemical decomposition of the energetic materials due to laser exposure, for each Raman spectrum, the laser beam was focused on the sample at a size of about 2 mm, then 10 Raman spectra of 5 s each were acquired at 3.0 mW laser power and averaged. ^{1}H and ^{13}C NMR spectra were measured at 400 MHz (Bruker AVANCE 400) with DMSO-d_6 as the solvent. High resolution mass spectra were performed on a Shimadzu LCMS-IT-TOF mass spectrometer using electrospray ionization (ESI). Elemental analysis was performed on a Vario Micro cube elemental analyzer. The detonation properties were calculated with Explo5 (version 6.02) software. The powder X-ray diffraction (XRD) patterns were recorded on a Bruker D8 Advance diffractometer, equipped with a Cu tube and Ni filter, yielding Cu $K_{\alpha1}$ and Cu $K_{\alpha2}$ radiation (λ_1 = 1–1.5406 Å, λ_2 = 1–1.5444 Å, respectively). The obtained diffraction patterns were refined by Rietveld method, as implemented within the program JADE 6.0, to determine the crystalline phase compositions and space groups. The structure analyses of typical qy-HMX crystals have been further performed under vacuum using Anton-paar SAX Sess mc2 system (SAXS) with Ni-filtered Cu Kα radiation (0.154 nm) operating at 50 kV and 40 mA at 25 ˚C. The β-HMX and δ-HMX lattice parameters as references for Rietveld refinement were adapted from JCPDS card No. 42–1768 and No. 44–1622, respectively. Gel permeation chromatography (GPC, Waters 2695) is a type of size exclusion chromatography (SEC) that separates analytes on the basis of size, which has been used to determine the content of TAGP dopants in each modified HMX crystals. The results and analytical method are presented in Fig. S13.

Performances: The crystal density was measured by two densitometers with a chamber size of 100 ml, filled with helium at a pressure of 0.5 MPa, where the sample mass for each test is about 1.0 gram. One has been measured by Gas Pycnometry Analyzer G-denpyc 2900 produced by Gold APP Instrument Corporation, and repeating experiments are done by equipment Micromeritics

Accupyc II 1340 gas pycnometer at 25 °C from another institute. The heat of combustion was measured in a calorimetry bomb filled with 3 MPa of pure oxygen, with a sample mass of about 1.0 gram for each test. The corresponding cylindrical of the charges that were used for heat of combustion tests are in a dimension of φ10 mm. Thermal analysis was performed on a Mettler Toledo instrument by thermogravimetric-differential scanning Calorimetry (TG–DSC). The samples were heated from 40 °C to 500 °C at a heating rate of 10 °C min^{-1} under Argon atmosphere. The heat of formation was calculated based on the following theory: The enthalpies of combustion were calculated according to the formula $\Delta_c H = \Delta_c U - \Delta nRT$, ($\Delta n = n_{(\text{gaseous products})} - n_{(\text{gaseous reactants})}$, R = 8.314 J mol^{-1} K^{-1} and T = 298.15 K) with the combustion products of CO_2, H_2O and N_2. The detonation velocity has been measured by a standard optical method, and the final result is the mean value of 25 measurements with the samples shown in Figure S17.

Single crystals structure results: A suitable crystal was selected and tested on a Bruker APX-II CCD diffractometer. The crystal was kept at 173 K during data collection. Using Olex2 (S1), the structure was solved with the ShelXT (S2) structure solution program, using Intrinsic Phasing and refined with the ShelXL (S3) refinement package with Least Squares minimisation. (1) Crystal Data for modified pure HMX $C_4H_8N_8O_8$ (M =296.18 g mol^{-1}): a = 6.527(5) Å, b = 10.926(7) Å, c = 8.699(7) Å, β = 124.59(2)°, V = 510.6(7) $Å^3$, Z = 2, T = 173 K, μ (MoKα) = 0.183 mm^{-1}, *Dcalc* = 1.926 g cm^{-3}, 4318 reflections measured (6.804° ≤ 2Θ ≤ 55.534°), 1193 unique (R_{int} = 0.0338, R_{sigma} = 0.0325) which were used in all calculations. The final R_1 was 0.0389 (I > 2σ(I)) and wR_2 was 0.1079 (all data). (2) Crystal Data for modified pure RDX, $C_3H_6N_6O_6$ (M =222.14 g mol^{-1}): orthorhombic, space group Pbca (no. 61), a = 11.545(4) Å, b = 10.663(3) Å, c = 13.185(4) Å, V = 1623.2(8) $Å^3$, Z = 8, T = 173 K, μ(Mo K_α) = 0.173 mm^{-1}, *Dcalc* = 1.818 g cm^{-3}, 7238 reflections measured (6.05° ≤ 2Θ ≤ 52.712°), 1645 unique (R_{int} = 0.0298, R_{sigma}= 0.0273) which were used in all calculations. The final R_1 was 0.0357 (I > 2σ(I)) and wR_2 was 0.1084 (all data).

S2 Supporting Figures and Tables

S2.1 Morphologies

β-HMX (Cream White) | HT-0 (Light grey) | HT-1 (Yellow) | HT-2 (Light Yellow)

HT-3 (Dark brown) | HT-4 (Grey) | HT-5 (Dark Grey) | HT-7 (Black)

Figure S1. Appearance photographs of the industrial grade β-HMX and various HMX crystals doped with 2D TAGP material.

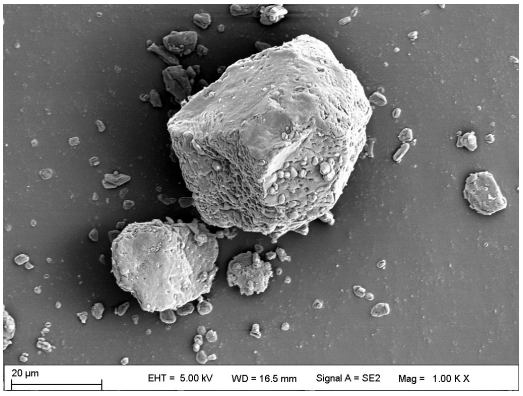

β-HMX (Industrial Grade)

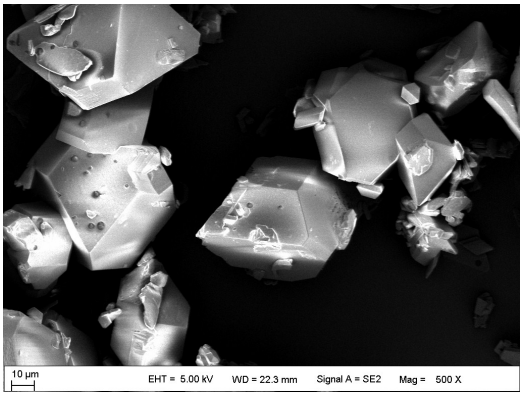

HT-0

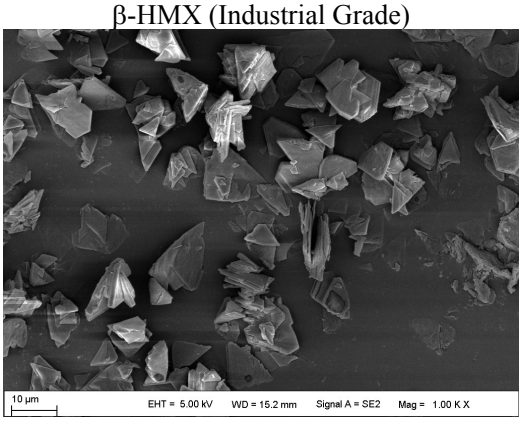

HT-1

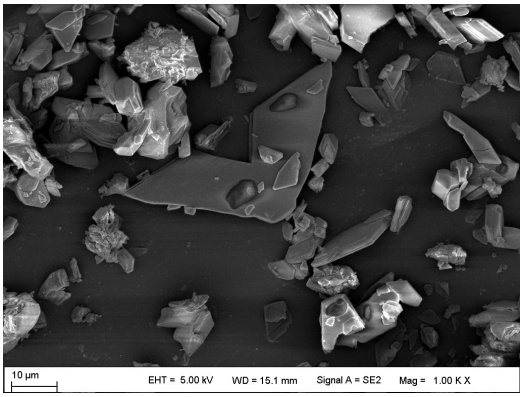

HT-2

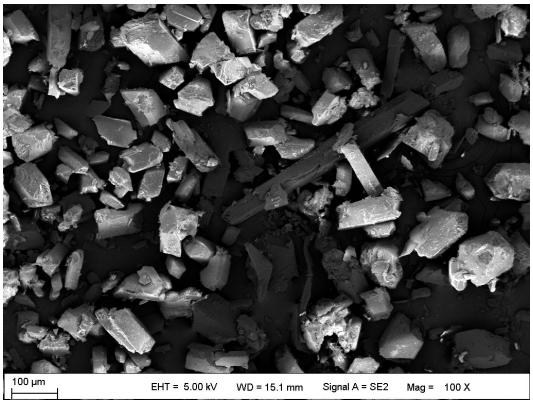

HT-3

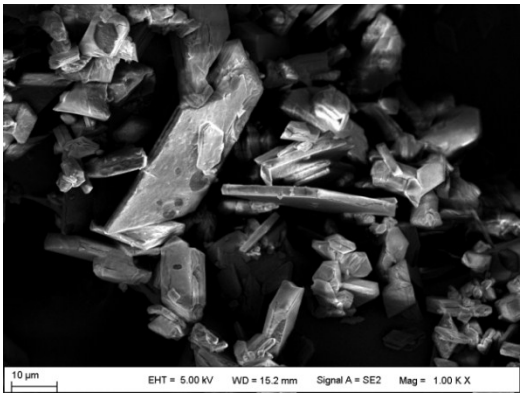

HT-4

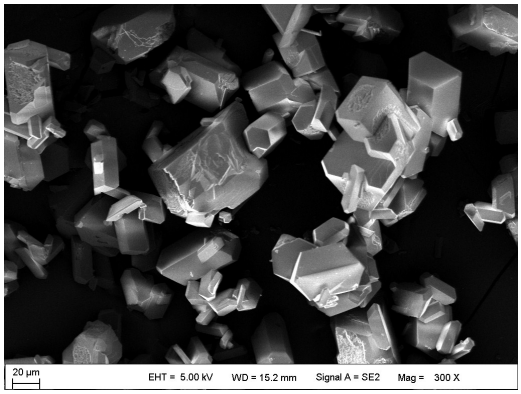

HT-5

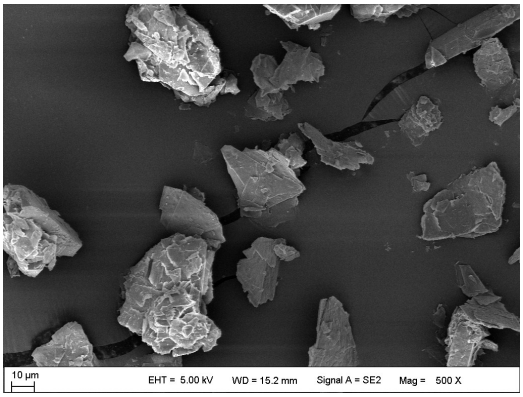

HT-7

Figure S2. SEM images of industrial grade β-HMX and various types of HMX crystals doped with TAGP 2D material.

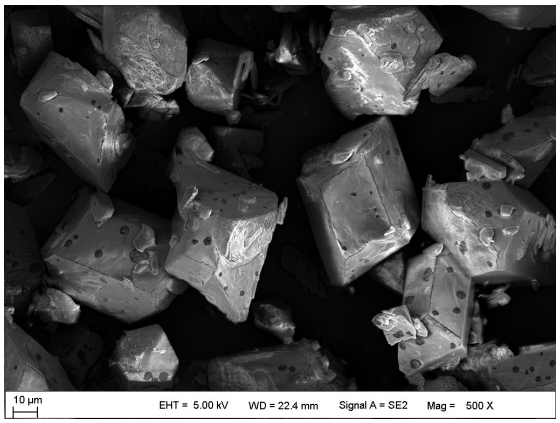

HT-0

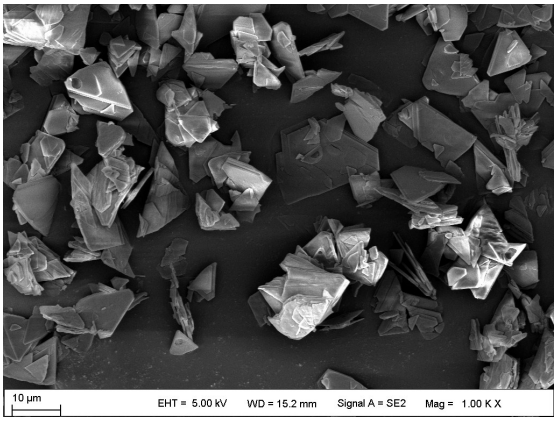

HT-1

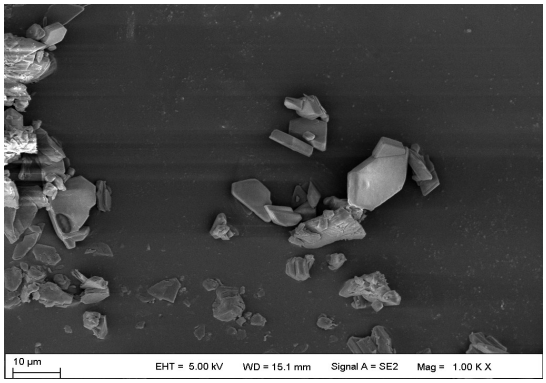

HT-2

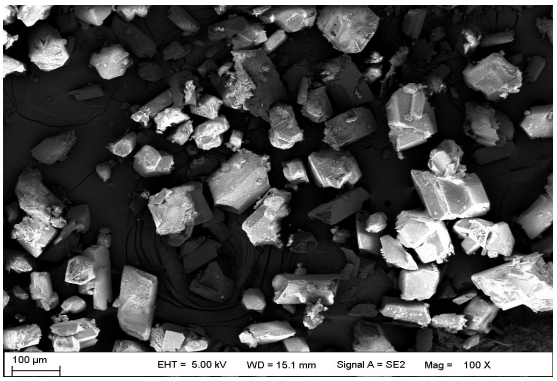

HT-3

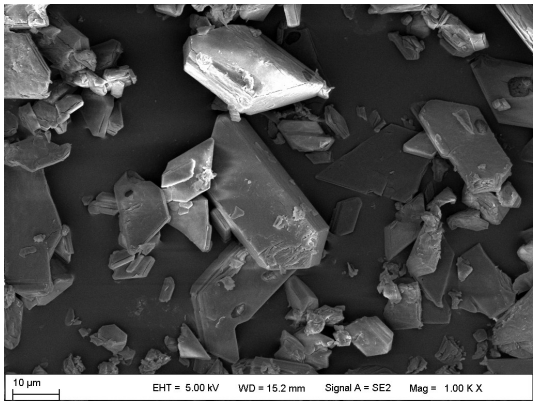

HT-4

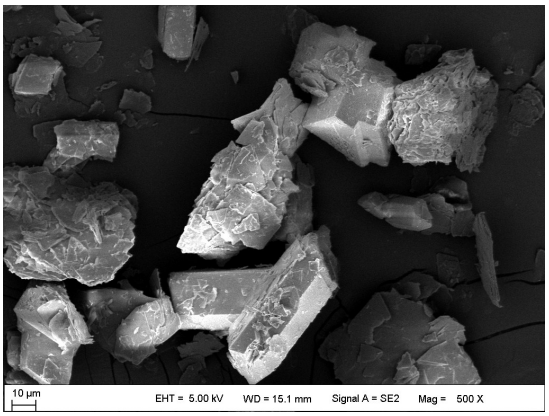

HT-7

Figure S2 (continued). SEM images of industrial grade β-HMX and various types of HMX crystals doped with TAGP 2D material.

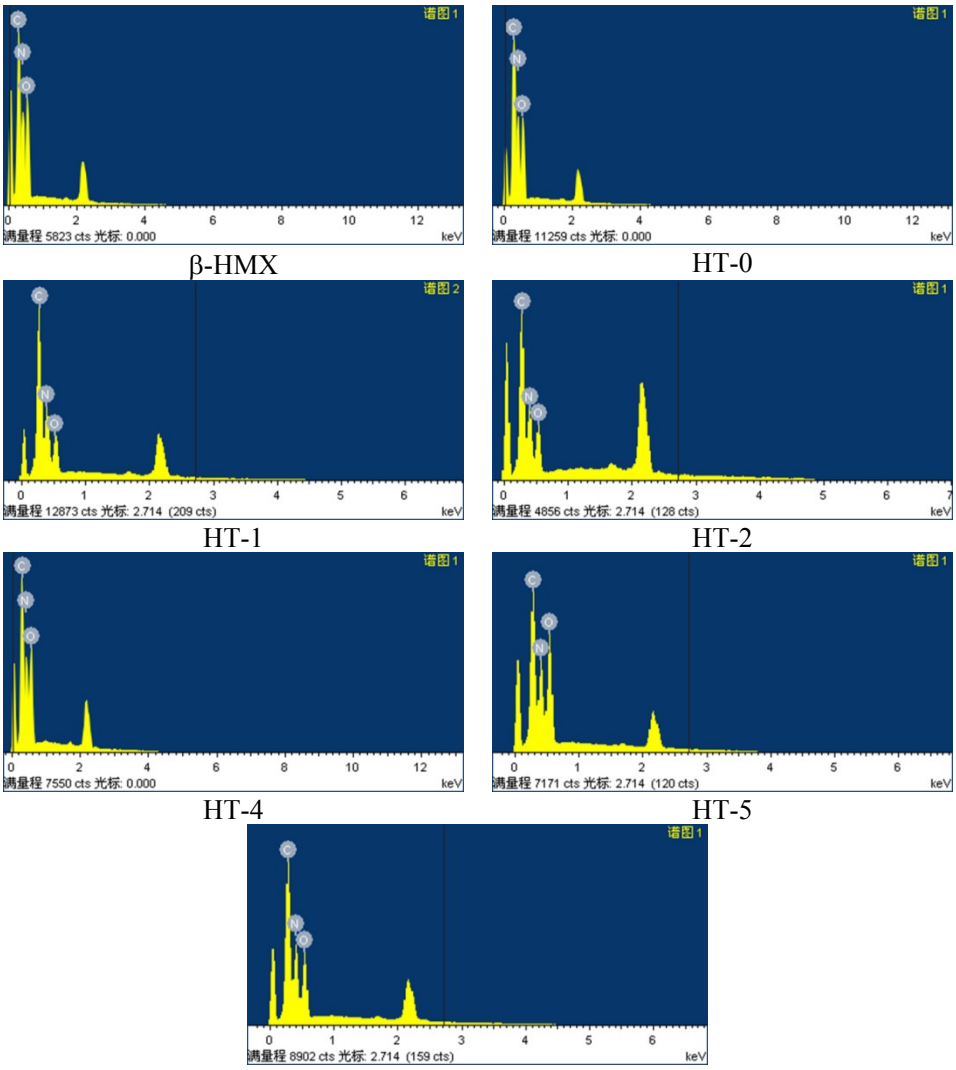

Figure S3. The EDS spectra of industrial grade β-HMX and HMX crystals doped with TAGP 2D material.

Table S1. Elemental content on the surfaces by EDS and the real elemental analyses by combustion method of industrial grade β-HMX and HMX crystals doped with TAGP

EDS method								
atom	β-HMX	HT-0	HT-1	HT-2	HT-3	HT-4	HT-5	HT-7
C K (%)	0.59	0.63	1.81	0.87	0.59	0.60	0.53	0.72
N K (%)	51.02	54.93	58.50	60.89	50.03	52.90	48.97	57.23
O K (%)	48.39	44.44	39.70	38.24	49.38	46.50	50.50	42.05
$N/O\ (\%)_e$	1.05:1	1.24:1	1.47:1	1.59:1	1.01:1	1.14:1	0.97:1	1.36:1
Combustion method (in wt.%)								
Sample	Weight (mg)	C	H	O	N	S	Experimental Formula	
HMX	theoretically	16.22	2.72	43.22	37.84	-	$C_4H_8O_8N_8$	
HMX	2.436	15.89	2.45	44.65	37.01	0	$C_4H_{7.35}O_{8.44}N_{7.99}$	
HT-0	2.271	15.95	2.43	44.85	36.77	0	$C_4H_{7.26}O_{8.44}N_{7.90}$	
HT-1	2.412	15.97	2.41	44.84	36.78	0	$C_4H_{7.20}O_{8.43}N_{7.90}$	
HT-4	2.332	16.02	2.45	44.74	36.79	0	$C_4H_{7.29}O_{8.39}N_{7.87}$	
HT-7	2.181	16.00	2.43	44.79	36.78	0	$C_4H_{7.24}O_{8.41}N_{7.88}$	

S2.2 Molecular and crystal structures

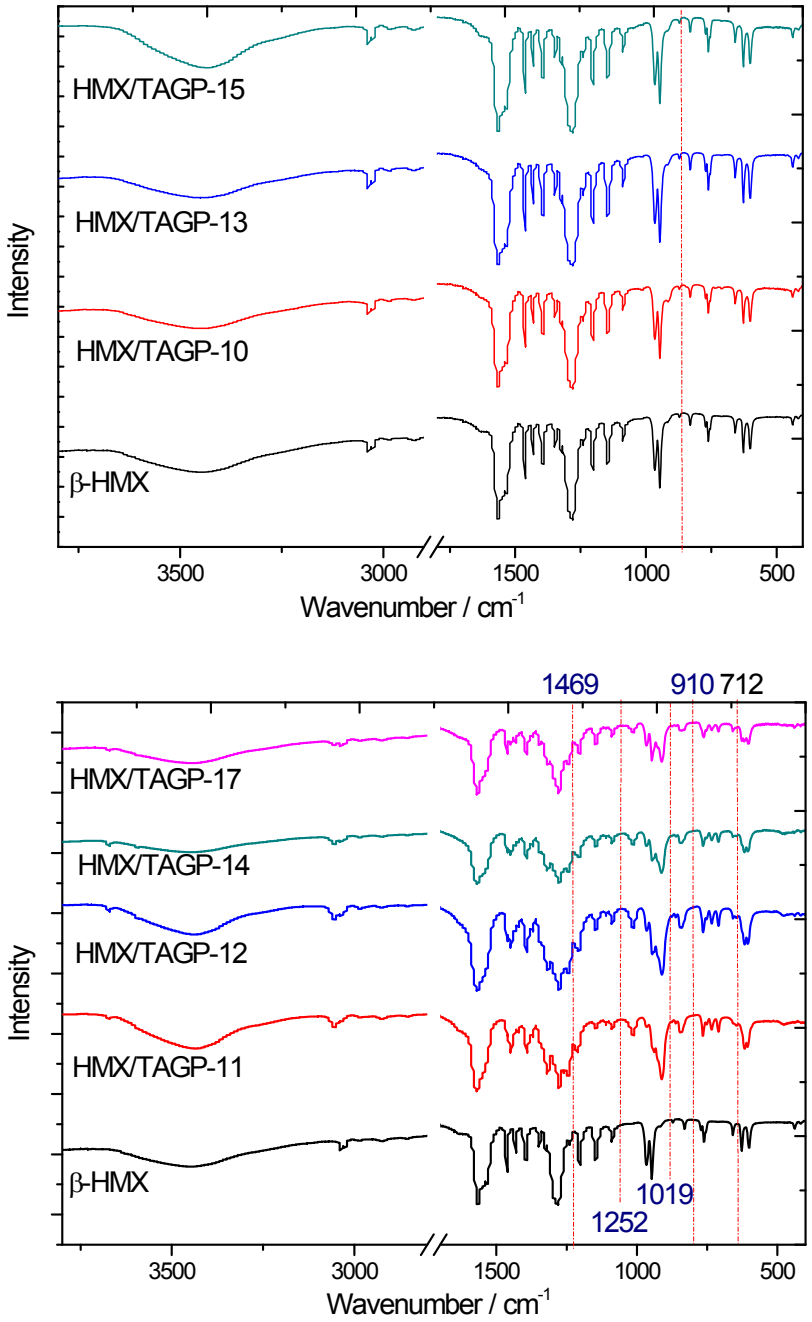

Figure S4. FTIR spectra of industrial grade β-HMX and HMX crystals doped with TAGP 2D material.

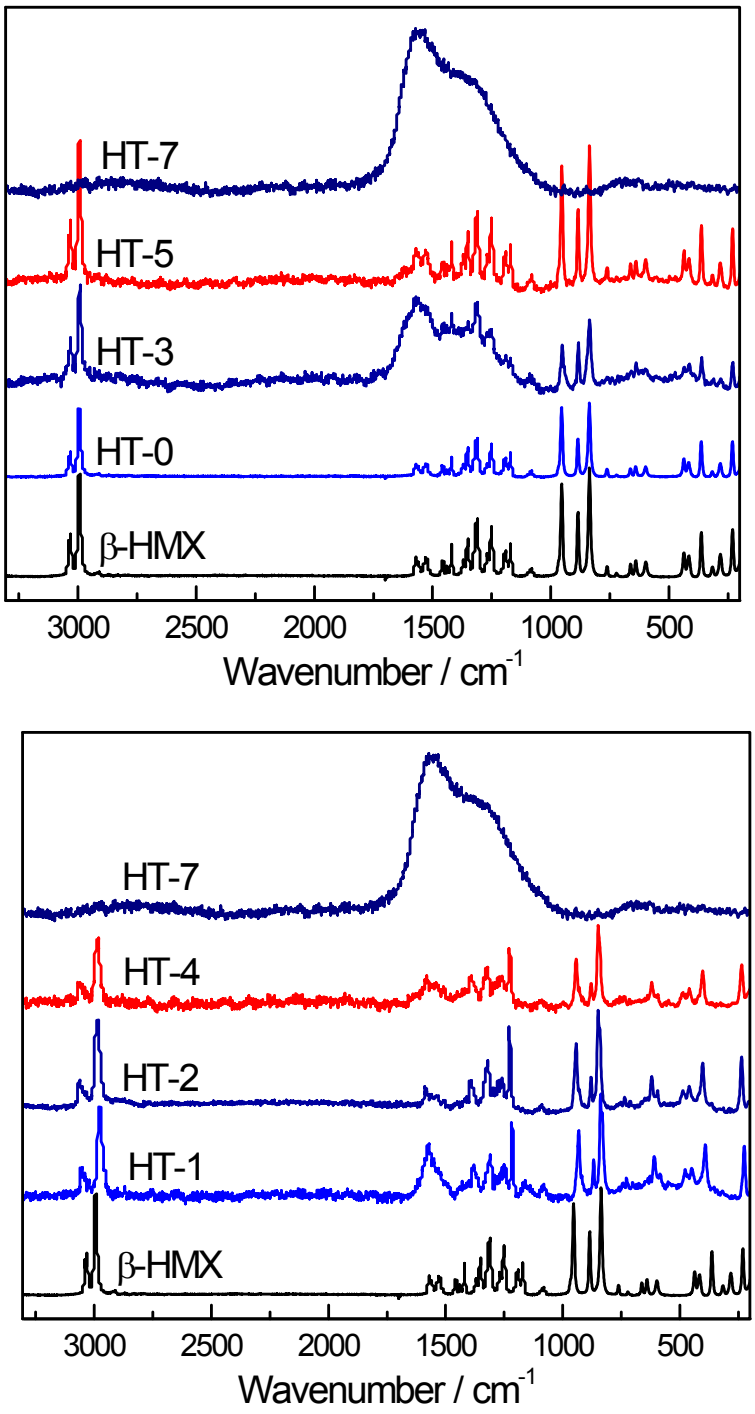

Figure S5. Raman spectra of industrial grade β-HMX and HMX crystals doped with TAGP 2D material.

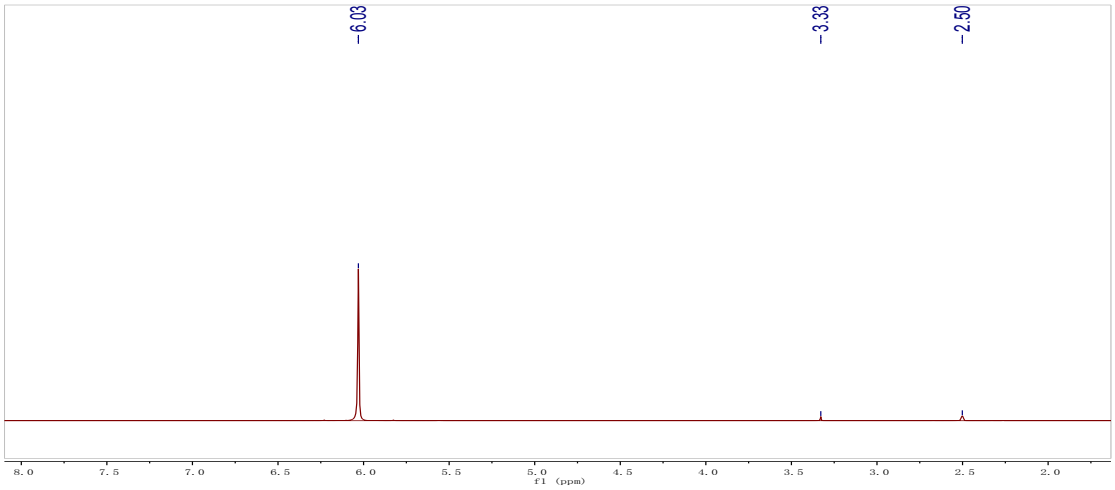

HMX ^{1}H NMR

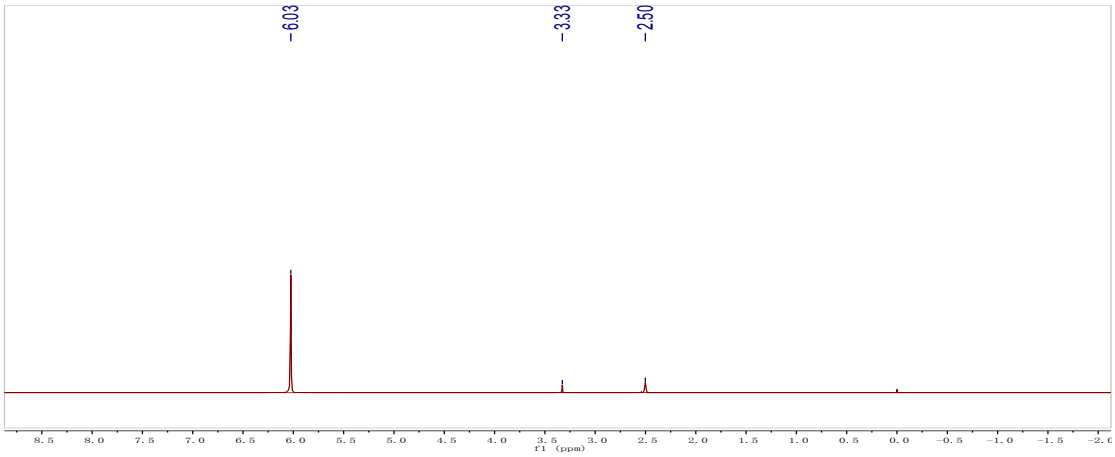

HT-4 ^{1}H NMR

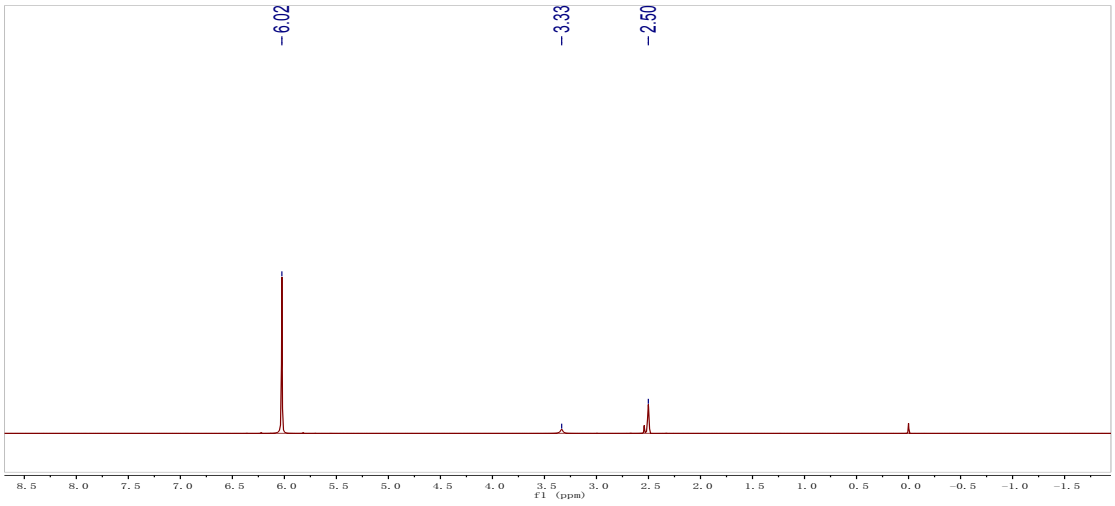

HT-7 ^{1}H NMR

Figure S6. A comparison of the ^{1}H NMR spectra of HMX, HT-4 and HT-7.

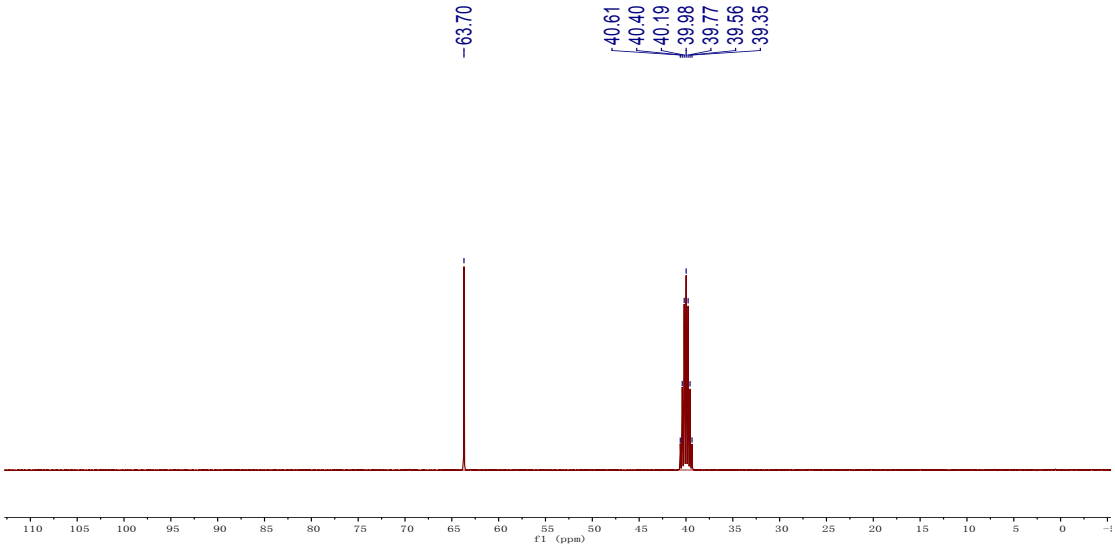

HMX ^{13}C NMR

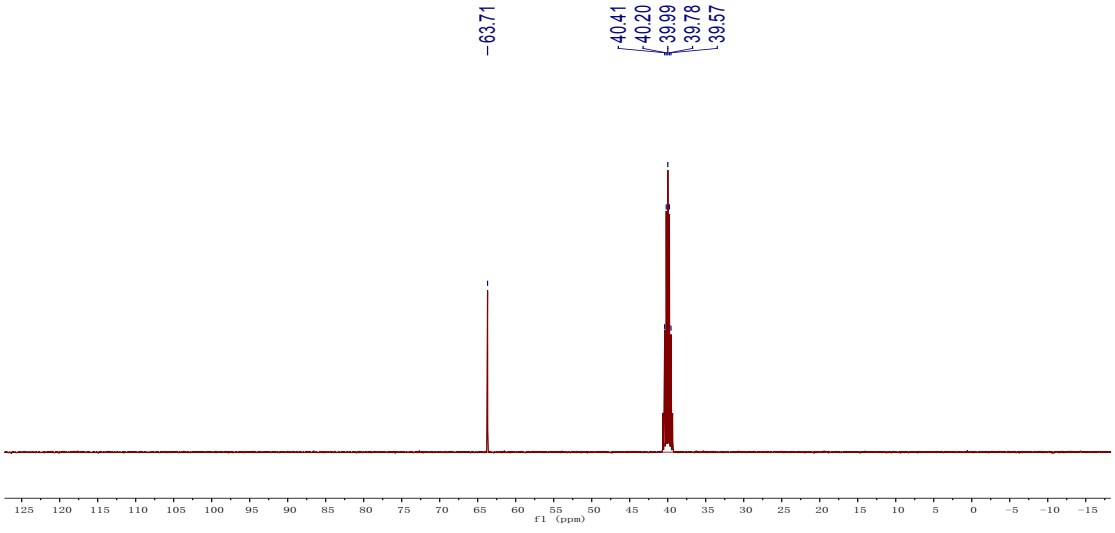

HT-4 ^{13}C NMR

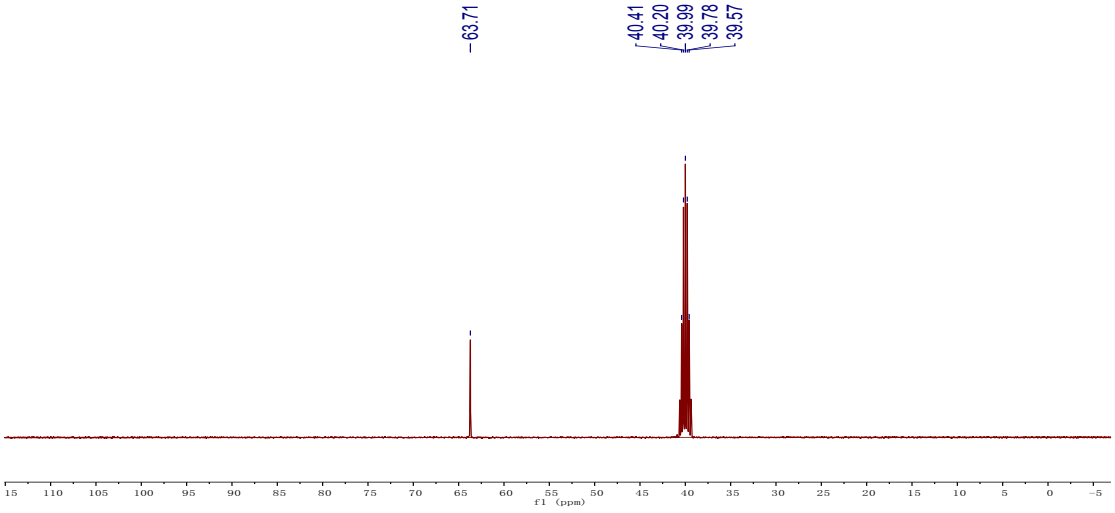

HT-7 ^{13}C NMR

Figure S7. A comparison of the ^{13}C NMR spectra of HMX, HT-4 and HT-7.

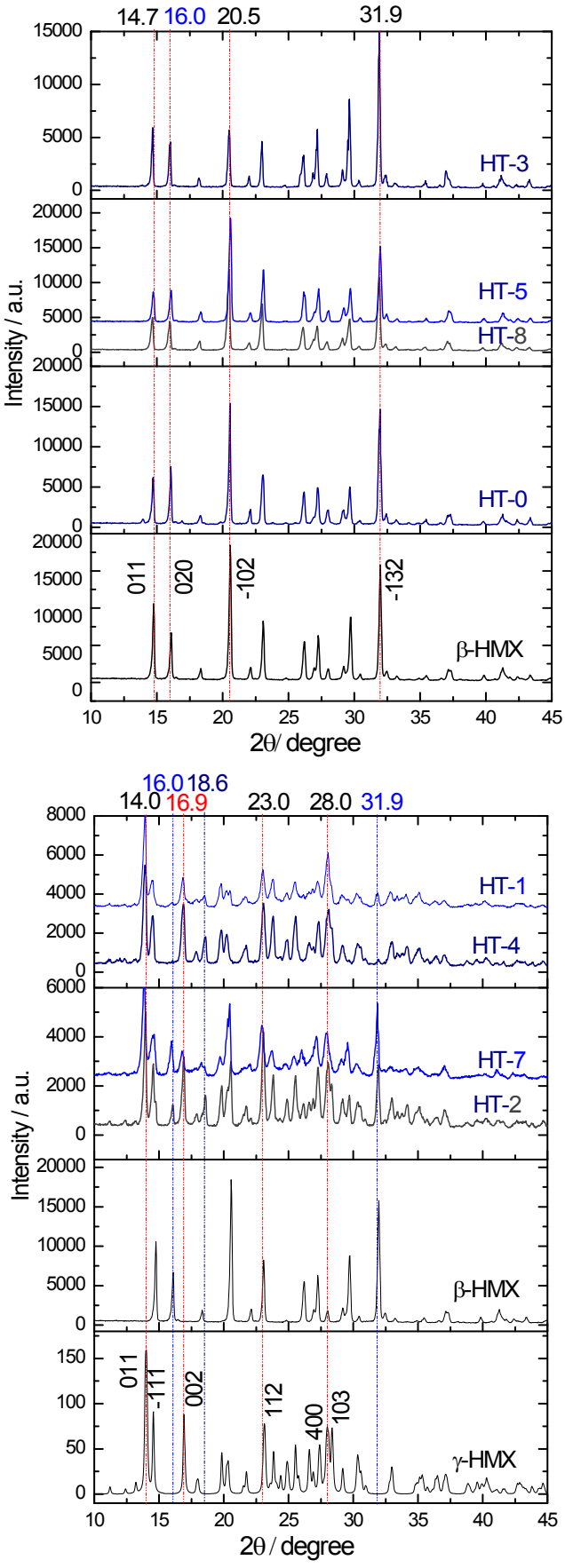

Figure S8. The PXRD spectra of various types of HMX crystals doped with TAGP 2D material, and they are compared with β-HMX and γ-HMX.

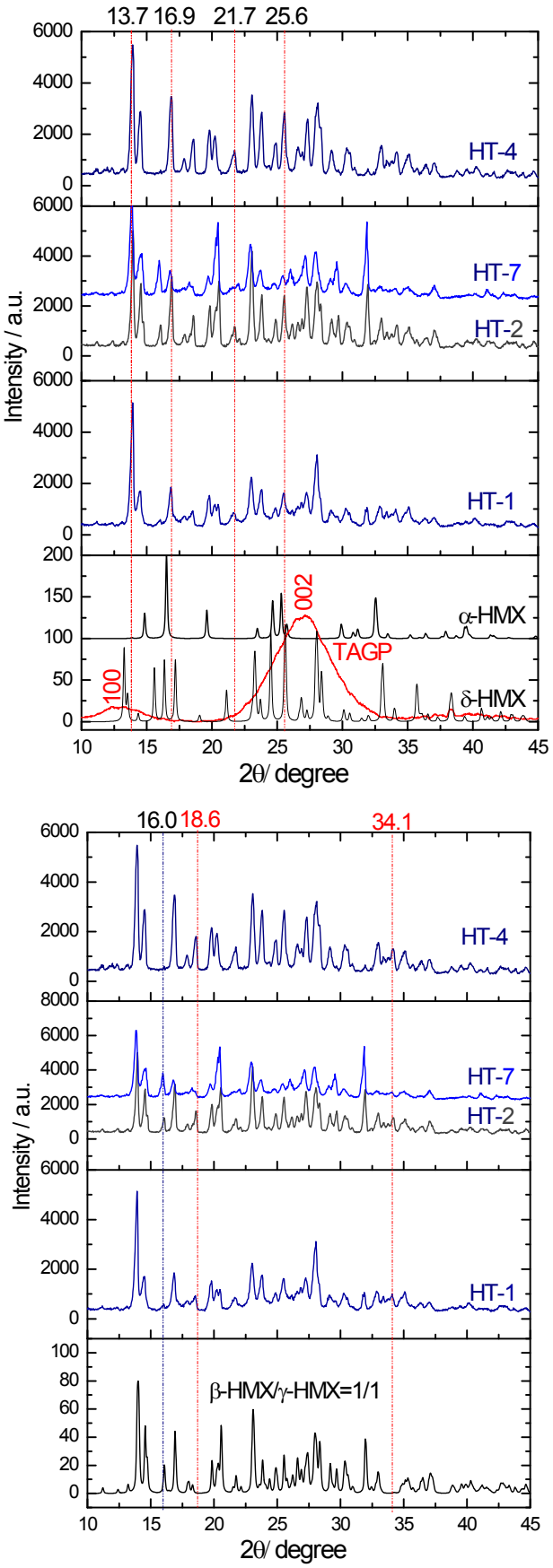

Figure S9. The PXRD spectra of various types of HMX crystals doped with TAGP 2D material, and they are compared with TAGP, α-HMX, δ-HMX and a mechanical mixture of β-HMX/γ-HMX.

Table S2. Parameters of hybrid crystalline HMX calculated value based on powder x-Ray data

Mater	**FOM**	**S-g**	**System**	***a***	***b***	***c***	***α***	**β**	***γ***	V_{cel}
β-HMX	Ex.	*P21/c* (14)	Mon-B	6.537	11.054	8.702	90°	124.4°	90°	518
γ-HMX	Ex.	*Pc* (7)	Mon-B	13.271	7.90	10.95	90°	106.8°	90°	1099
HT-0	8	*Cc* (9)	Mon-B	6.221	11.934	12.74	90°	97.5°	90°	937
HT-1	25	*Cc* (9)	Mon-B	7.197	15.953	19.13	90°	93.9°	90°	2191
HT-2	23	*Pban* (50)	Othorh	7.394	15.321	18.606	90°	90°	90°	2108
HT-3	13	*Pc* (7)	Mon-B	7.184	5.416	13.158	90°	123.0°	90°	430
HT-4	25	*C2* (5)	Mon-B	13.908	8.878	16.886	90°	110.3	90°	1956
HT-5	19	*P21/c* (14)	Mon-B	6.526	11.024	8.693	90°	124.5°	90°	516
HT-7	9	*P1* (1)	Triclinic	11.984	12.005	10.406	45°	131.7°	145°	595

Notes: S-g, Space group; Othorh, means orthorhombic; Ex., Experimental values by single crystal x-ray diffraction;; Mon-B, Monoclinic-B; a, b, c are crystal lattice parameters, in Å; V_{cel}, volume of the cell, in Å^3.

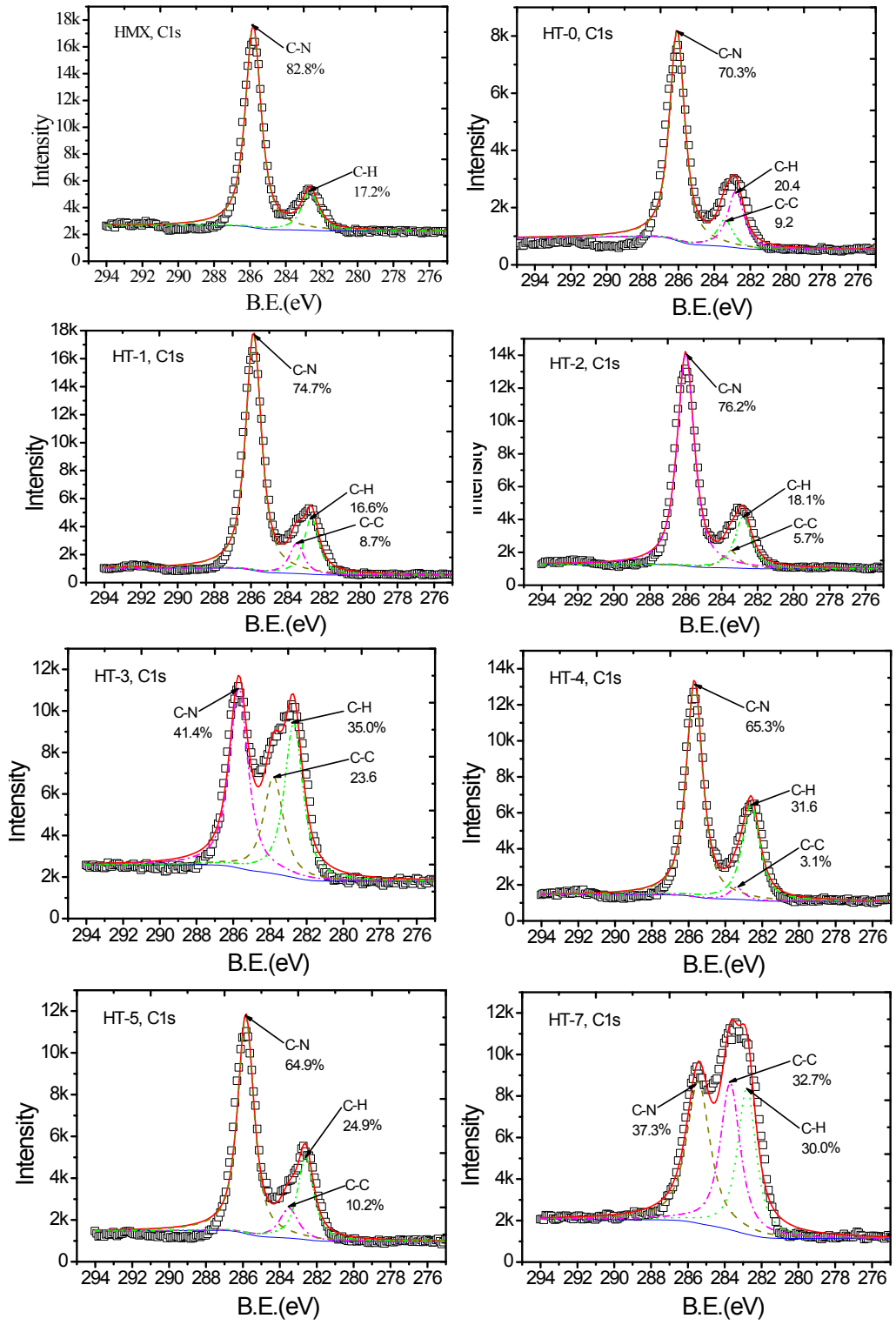

Figure S10. The C1s spectra of industrial grade β-HMX and HMX crystals doped with TAGP 2D material with peak separations.

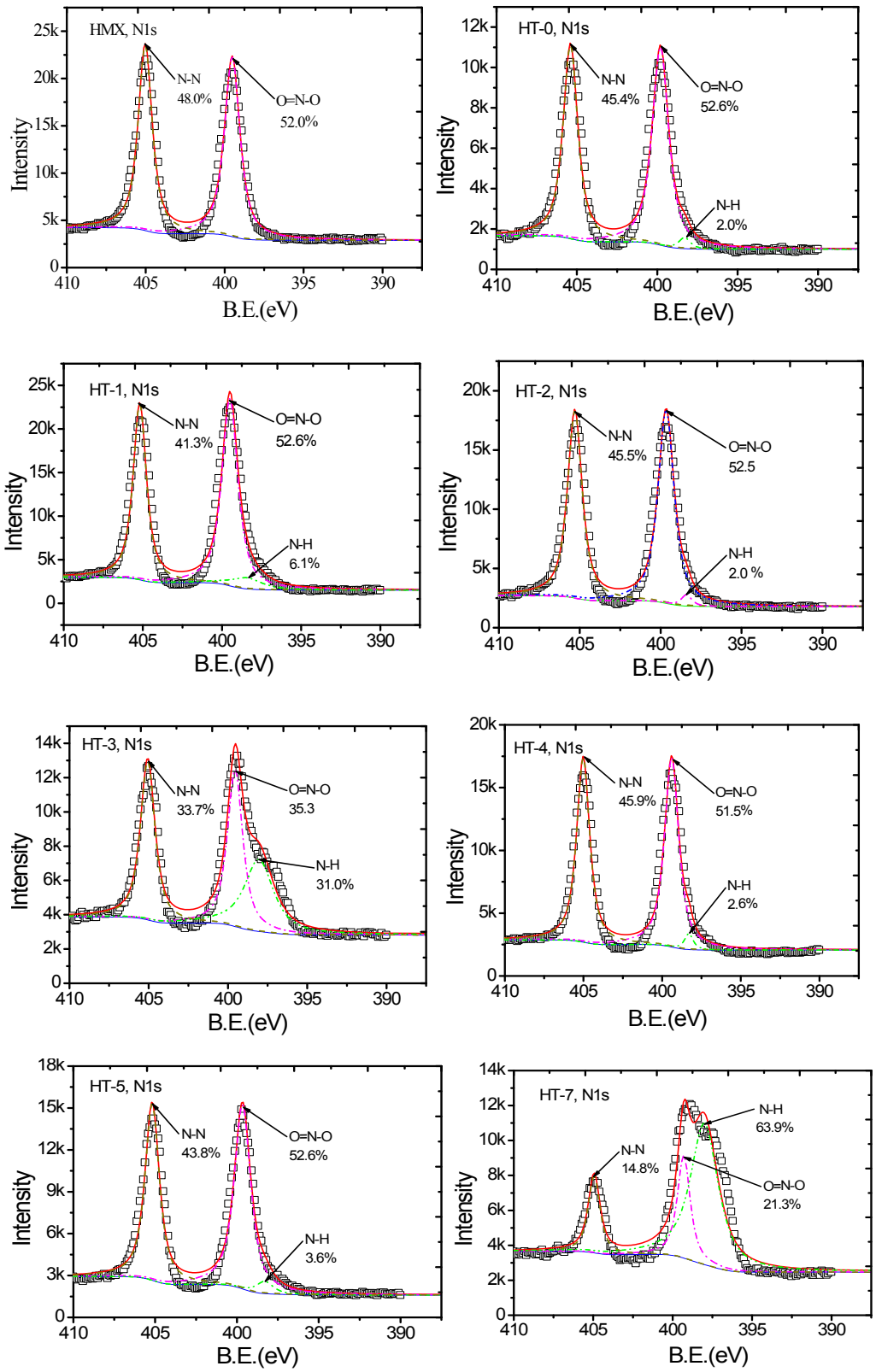

Figure S11, The N 1s spectra of industrial grade β-HMX and HMX crystals doped with TAGP 2D material with peak separations.

Table S3, Elemental content from XPS spectra of industrial grade β-HMX and HMX crystals doped with TAGP 2D material

atom	β-HMX	HT-0	HT-1	HT-2	HT-3	HT-4	HT-5	HT-7
C 1s (%)	27.42	30.01	29.76	29.72	42.01	32.83	32.87	49.3
N 1s (%)	37.04	37.86	38.91	37.58	29.83	35.21	36.43	30.69
O 1s (%)	35.54	32.13	31.33	32.7	27.22	31.97	30.69	19.35
S 2p	0	0	0	0	0.95	0	0	0.66
$C/N\ (\%)_e$	0.74:1	0.79:1	0.76:1	0.79:1	**1.41**:1	0.93:1	0.90:1	**1.61**:1

XPS analysis was performed to investigate the surface chemistry of the HMX crystals in order to confirm the effectiveness of the doping process. Representative high-resolution spectra of the C 1s, O 1s, and N 1s regions, obtained from HMX and the doped HMX crystals are shown in Figs. S10 and S11. To obtain the fine signatures from the XPS spectra, elemental core-level spectra were fit using the Avantage XPS software provided by XPS manufacturer. After the subtraction of Shirley background for N 1s, O 1s, and C 1s peaks, the percent contribution of C 1s, O 1s, and N 1s atom for these materials were integrated and presented in Table S3. About 0.66% and 0.95% atomic content of Sulfite has been found in the sample HT-17 and HT-13, respectively, according to XPS analysis. It is due to a minor inclusion of the fragments containing S atom in the crystal structure from the dissociated DMSO as a solvent under high temperature. In HMX molecular structure, elemental nitrogen has two chemical states with equal molar ratio. Therefore, the intensity of N*-N and N*-O peak is almost the same theoretically. All spectra were fit by a convolution of Gaussian and Lorentzian line at a ratio of 70:30. The binding energies, assigned chemical groups, and corresponding percent contribution of each peak are marked in Figs. S10 and S11. For the HMX, the C 1s region was fitted to two peaks, assigned to N-C−N and CH_2 species. The N 1s region of HMX can be fitted to two peaks at 399.6 eV and 400.3 eV, which are attributed to the nitro-nitrogen (–N–NO_2) and amine-nitrogen bonds (–N–C) of the HMX molecule, respectively.

Raman spectroscopy is known as a non-destructive method of characterizing organic chemicals. As shown in Fig. S5, HMX displays a fingerprint-like quality of β-HMX in the region of 200–600 cm^{-1}. Peaks in the 800–960 cm^{-1} regions are attributed to the ring-stretching vibration of HMX molecules. The peaks from 1000 to 1500 cm^{-1} region are due to the symmetric vibrational stretching of the NO_2 and N–N groups in HMX, whereas the 1500–1650 cm^{-1} regions corresponds to the asymmetric vibration of the NO_2 group. The peaks in the region of 2900–3300 cm^{-1} are ascribed to the symmetric and asymmetric CH_2 vibrations in the HMX molecule.

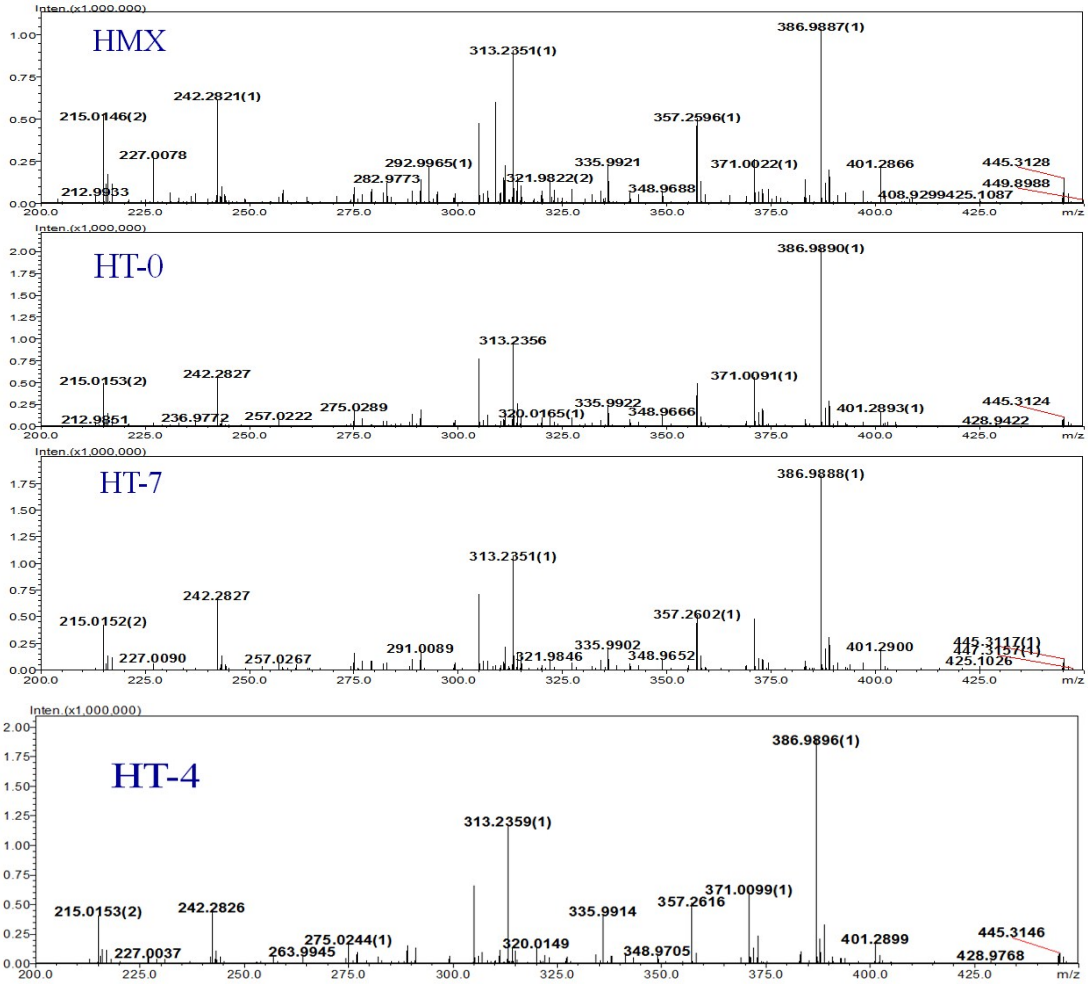

Figure S12. The high resolution MS of industrial grade β-HMX and various HMX crystals doped with TAGP 2D material

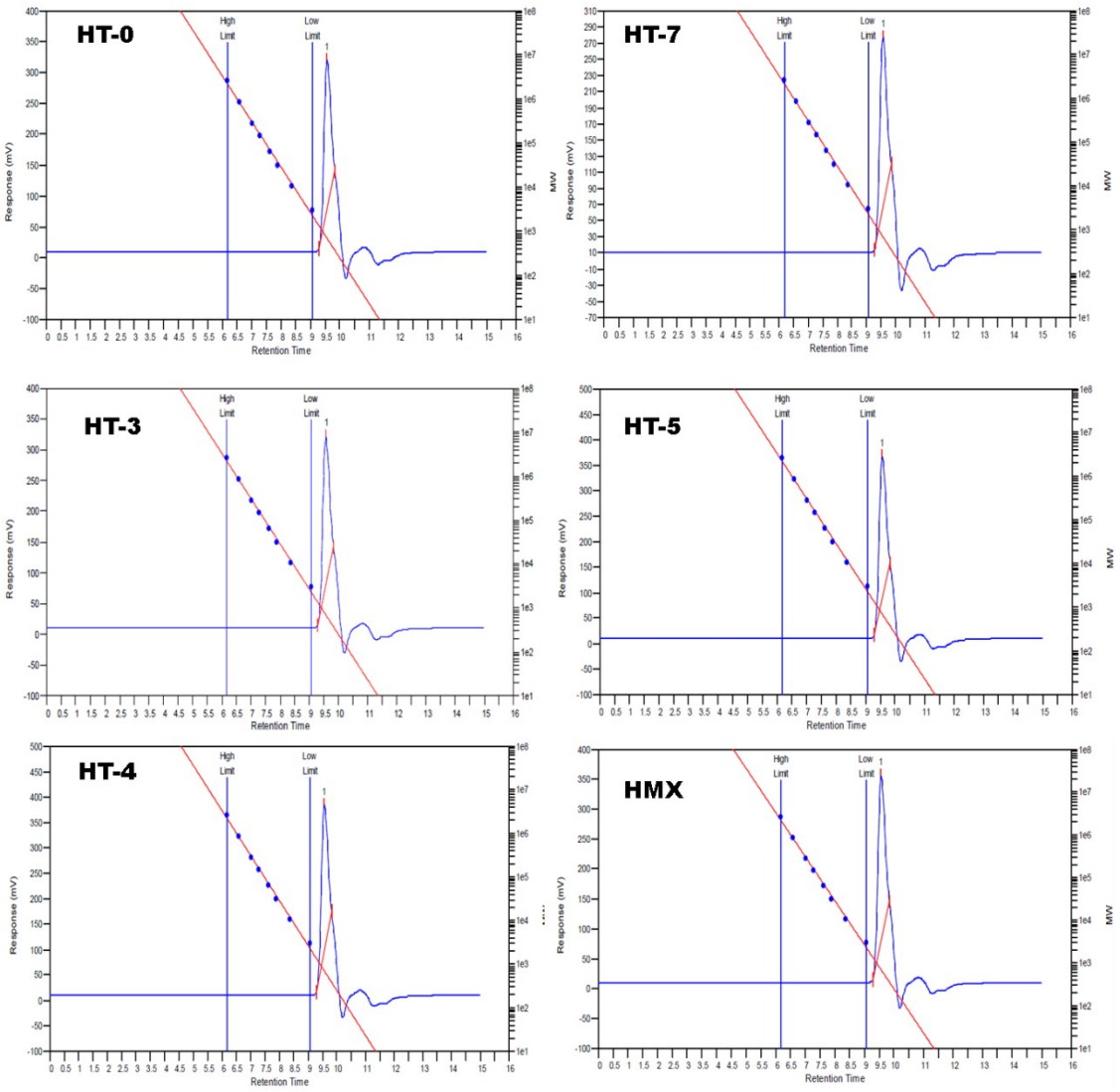

Name	Start RT (mins)	Max RT (mins)	End RT (mins)	Height (mV)	Area (mV.secs)	HMX content % Area
HMX	9.2833	9.5667	9.85	274.82	4328.49	100.00
HT-0	9.2833	9.5667	9.83	240.31	3677.13	84.95
HT-3	9.2833	9.5833	9.83	237.11	3681.48	85.05
HT-4	9.2833	9.5667	9.82	284.18	4243.58	98.04
HT-5	9.2833	9.5667	9.83	278.80	4299.56	99.33
HT-7	9.2833	9.5667	9.85	209.50	3260.95	75.33

Figure S13. The GPC curves of industrial grade β-HMX and HMX crystals doped with TAGP 2D material, based on which the exact content of HMX molecules in each sample were determined based on the reference pure HMX crystal (integration of the distribution peaks). The experimental conditions are as follows: Concentration, 0.10 mg ml^{-1}; K of Sample, 14.1000; Injection Volume, 100.0 ul; Alpha of Sample, 0.7000; Eluent, DMF Flow Rate, 1.00 ml min^{-1}; Column Set Length, 350 mm; Temperature, 80 ˚C.

Table S4 Crystal data and structure refinement for qy-HMX and normal HMX from literature

Empirical formula	$C_4H_8N_8O_8$	$C_4H_8N_8O_8$
Formula weight	296.18	296.18
Temperature / K	173	173
Crystal system	monoclinic	monoclinic
Space group	P21/c	P21/c
a/Å	6.527(5)	6.5370(8)
b/Å	10.926(7)	11.054(2)
c/Å	8.699(7)	8.7018(22)
α/°	90	90
β/°	124.59(2)	124.44(3)
γ/°	90	90
Volume / $Å^3$	510.6(7)	518.56
Z	2	2
ρ_{calc} / g cm^{-3}	1.926	1.897
μ / mm^{-1}	0.183	-
F(000)	304.0	-
Crystal size / mm^3	0.22 × 0.2 × 0.18	-
Radiation	Mo Kα (λ = 0.71073)	Cu Kα (λ = 1.5418)
2Θ range for data collection/°	6.804 to 55.534	-
Index ranges	$-8 \le h \le 6$, $-12 \le k \le 14$, $-11 \le l \le 11$	-
Reflections collected	4318	-
Independent reflections	1193 [R_{int} = 0.0338, R_{sigma} = 0.0325]	-
Data/restraints/parameters	1193/0/91	-
Goodness-of-fit on F^2	1.116	-
Final R indexes [I>=2σ (I)]	R_1 = 0.0389, wR_2 = 0.1019	-
Final R indexes [all data]	R_1 = 0.0438, wR_2 = 0.1079	-
Largest diff. peak/hole / e $Å^{-3}$	0.28/-0.38	-
Reference	This paper	[S4, S5]

Table S5. Fractional Atomic Coordinates ($\times 10^4$) and Equivalent Isotropic Displacement Parameters ($Å^2 \times 10^3$) for squeezed HMX. U_{eq} is defined as 1/3 of the trace of the orthogonalised U_{IJ} tensor.

Atom	*x*	*y*	*z*	U(eq)
O3	7721.6(18)	7203(1)	4357.2(15)	26.5(3)
O4	6413.2(19)	7481.6(10)	6830.6(16)	30.0(3)
O2	7731(2)	5710.8(10)	767.6(15)	30.2(3)
O1	9657.6(17)	4390.8(10)	2626.8(16)	29.0(3)
N3	4813.9(18)	6231.8(10)	4604.1(15)	15.1(3)
N2	6428.6(19)	4740.6(10)	2936.4(15)	18.4(3)
N4	6408(2)	7035.1(10)	5301.4(17)	18.7(3)
N1	8030(2)	4978.1(11)	2065.9(16)	20.6(3)
C1	4782(2)	5651.9(12)	2806.9(18)	17.4(3)
C2	3094(2)	6158.9(12)	5526.9(18)	17.7(3)

Table S6. Anisotropic Displacement Parameters ($Å^2 \times 10^3$) for squeezed HMX. The Anisotropic displacement factor exponent takes the form: $-2\pi^2[h^2a^{*2}U_{11}+2hka^*b^*U_{12}+\ldots]$.

Atom	U_{11}	U_{22}	U_{33}	U_{23}	U_{13}	U_{12}
O3	22.9(6)	28.7(6)	29.9(6)	3.2(4)	9.8(4)	-8.3(4)
O4	32.7(7)	29.4(6)	27.8(6)	-13.4(4)	6.3(5)	-8.9(5)
O2	40.5(7)	30.1(6)	24.2(6)	3.1(4)	16.5(5)	-3.1(5)
O1	17.2(6)	36.9(6)	34.9(6)	-2.5(5)	9.9(4)	0.8(4)
N3	13.7(6)	14.8(5)	17.3(5)	-2.0(4)	4.1(4)	-2.2(4)
N2	18.5(6)	19.6(6)	18.9(5)	2.0(4)	8.0(4)	2.0(5)
N4	18.1(6)	15.1(5)	22.2(6)	0.6(4)	2.9(5)	-2.0(4)
N1	21.4(7)	22.3(6)	19.9(6)	-5.5(4)	8.7(5)	-5.0(5)
C1	18.3(7)	18.2(6)	14.7(6)	-0.2(4)	1.7(5)	1.4(5)
C2	16.1(7)	17.7(6)	19.5(6)	1.0(5)	4.7(5)	1.4(5)

Table S7 Bond Lengths for squeezed HMX.

Atom	Atom	Length/Å	Atom	Atom	Length/Å
O3	N4	1.2272(18)	N3	C2	1.4333(18)
O4	N4	1.2225(18)	N2	N1	1.3623(18)
O2	N1	1.2269(17)	N2	C1	1.4528(19)
O1	N1	1.2332(18)	N2	C2[1]	1.4770(18)
N3	N4	1.3724(17)	C2	N2[1]	1.4770(18)
N3	C1	1.4587(18)			

[1]1-X,1-Y,1-Z

Table S8. Bond Angles for squeezed HMX.

Atom	Atom	Atom	Angle/°	Atom	Atom	Atom	Angle/°
N4	N3	C1	118.41(11)	O4	N4	O3	126.47(13)
N4	N3	C2	117.88(11)	O4	N4	N3	116.66(12)
C2	N3	C1	122.92(11)	O2	N1	O1	125.38(13)
N1	N2	C1	118.05(11)	O2	N1	N2	118.62(13)
N1	N2	C2[1]	115.32(11)	O1	N1	N2	115.94(12)
C1	N2	C2[1]	122.48(10)	N2	C1	N3	111.90(11)
O3	N4	N3	116.82(12)	N3	C2	N2[1]	109.86(11)

[1]1-X,1-Y,1-Z

Table S9. Torsion Angles for squeezed HMX.

A	B	C	D	Angle/°	A	B	C	D	Angle/°
N4	N3	C1	N2	71.88(15)	C1	N2	N1	O1	159.70(11)
N4	N3	C2	N2[1]	-87.55(14)	C2	N3	N4	O3	-170.70(11)
N1	N2	C1	N3	-111.74(13)	C2	N3	N4	O4	11.59(17)
C1	N3	N4	O3	-0.60(17)	C2	N3	C1	N2	-118.55(14)
C1	N3	N4	O4	-178.31(11)	C2[1]	N2	N1	O2	179.48(11)
C1	N3	C2	N2[1]	102.83(14)	C2[1]	N2	N1	O1	1.99(16)
C1	N2	N1	O2	-22.80(17)	C2[1]	N2	C1	N3	44.29(17)

[1]1-X,1-Y,1-Z

Table S10. Hydrogen Atom Coordinates (Å×10^4) and Isotropic Displacement Parameters (Å^2×10^3) for squeezed HMX.

Atom	*x*	*y*	*z*	U(eq)
H1A	3402	5257	2349	21
H1B	4962	6286	1890	21
H2A	1806	5910	4622	21
H2B	2842	6972	6031	21

S2.3 Properties and Performances

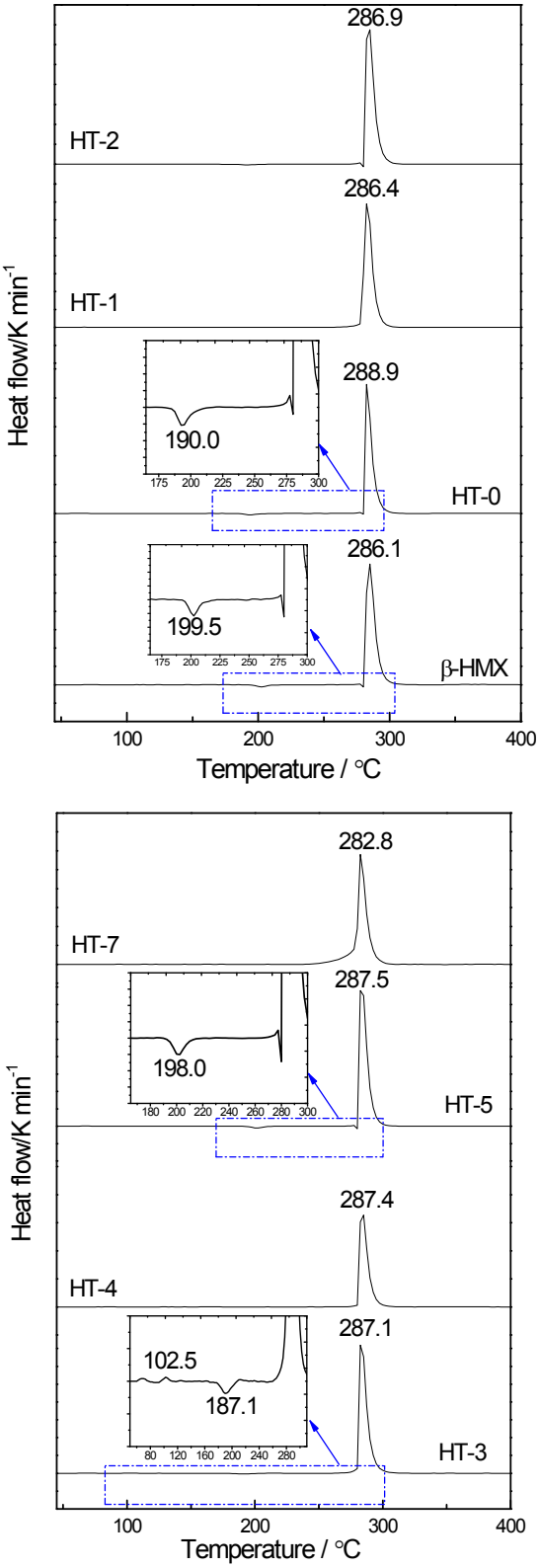

Figure S14. The non-isothermal DSC curves of industrial grade β-HMX and various HMX crystals doped with TAGP 2D material at a heating rate of 5 °C min^{-1}.

The DSC curve of HMX shows three peaks, the weak endothermic peak at about 195 °C is due to the morphology transformation, after the transformation the sharp endothermic peak at 281 °C corresponds to melting which is followed by strong exothermic peaks, this peak immediately after the melting is due to the self-decomposition of HMX (S6). A contraction of β - HMX was found before changing into δ - HMX resulting in a high volume difference during the transition. The final reconversion results in mixtures of α− and β-HMX (S7, S8). The successful doping of TAGP between the crystal lattice of HMX would result in no polymorphic transition during heating (Fig. S14).

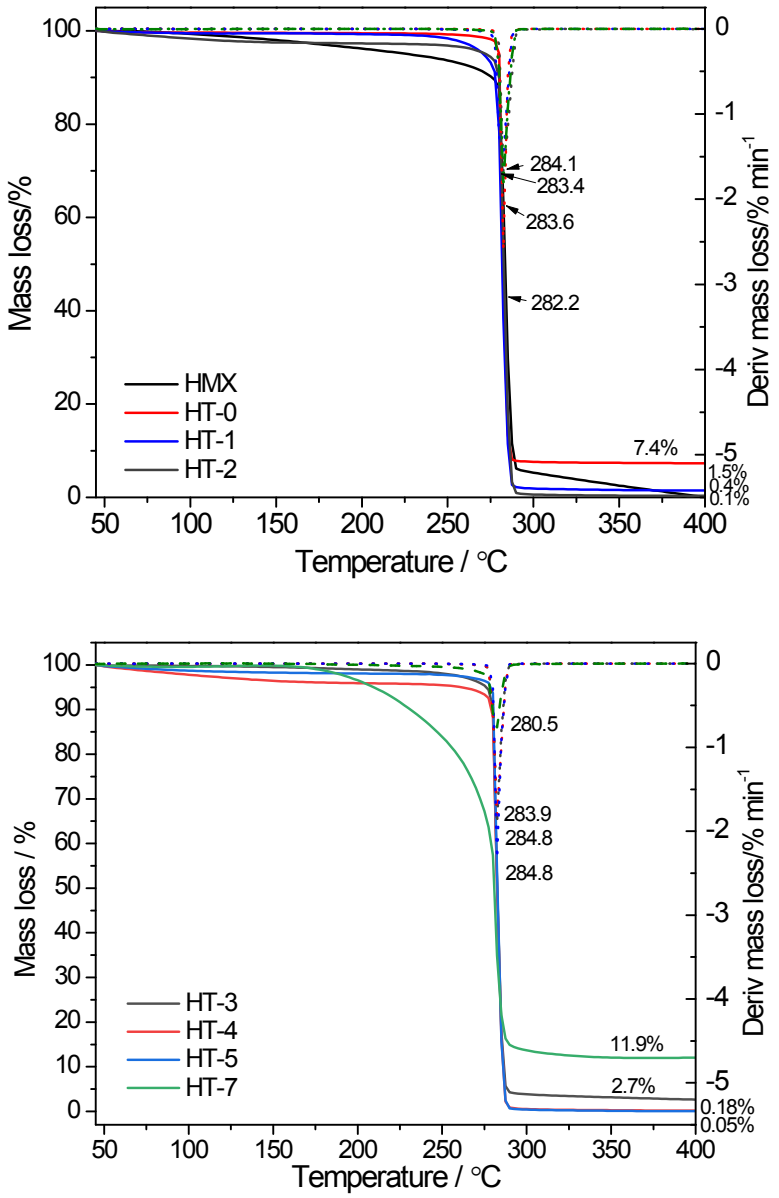

Figure S15. The non-isothermal TG curves of industrial grade β-HMX and various HMX crystals doped with TAGP 2D material at a heating rate of 5 °C min^{-1}.

Table S11. The original experimental records from the densitometer using Helium as the filling gas.

No. of Tests	Samples	HMX	HT-0	HT-1	HT-2
	Average (g cm^{-3})	1.884	1.620	1.841	1.839
	Uncertainty(±g cm^{-3})	0.005	0.003	0.003	0.005
1		1.886410	1.610430	1.840728	1.853045
2		1.907882	1.620669	1.846562	1.857609
3		1.874945	1.620387	1.859863	1.845966
4		1.871631	1.616943	1.822724	1.849562
5		1.881520	1.623249	1.833397	1.833582
6		1.912747	1.610671	1.836728	1.801305
7		1.882781	1.617535	1.851837	1.860464
8	Density, in g cm^{-3}	1.849002	1.630333	1.834176	1.817640
9		1.882070	1.630966	1.838632	1.845179
10		1.896185	1.600349	1.848247	1.849770
11		1.896076	1.605699	1.851769	1.840292
12		1.876185	1.613431	1.831966	1.818975
13		1.892453	1.639699	1.842981	1.824994
14		1.898986	1.629397	1.844676	1.870182
15		1.854009	1.632882	1.829914	1.822111
Tested sample mass, in mg		1052.90	631.32	1009.38	1025.09
No. of Tests	Samples	HT-3	HT-4	HT-5	HT-7
	Average (g cm^{-3})	1.934	2.040	1.868	2.131
	Uncertainty (±g cm^{-3})	0.005	0.004	0.006	0.008
1		1.925807	2.059565	1.883507	2.124510
2		1.940123	2.053626	1.845357	2.123653
3		1.905984	2.048556	1.883006	2.185538
4		1.945171	2.055036	1.893305	2.112723
5		1.904108	2.058969	1.824307	2.131794
6		1.957898	2.052189	1.872434	2.111522
7		1.947763	2.037817	1.882994	2.088730
8	Density, in g cm^{-3}	1.936914	2.019926	1.869070	2.151188
9		1.942138	2.026080	1.854606	2.157422
10		1.925929	2.025606	1.828143	2.112095
11		1.913108	2.030601	1.891993	2.185321
12		1.931880	2.023642	1.880085	2.077889
13		1.947673	2.036647	1.878189	2.176885
14		1.961807	2.038523	1.866203	2.103006
15		1.921613	2.029920	1.872439	2.126517
Tested sample mass, in mg			677.44	1052.90	1008.97

Table S12. The non-isothermal TG/DTG data of different HMX crystals doped with TAGP material.

		TG curves			DTG peaks			Residue
Samples	β	T_i/°C	T_{ot}/°C	Mass loss	L_{max}	T_p/°C	T_{oe}/°C	(%)

β-HMX	10	241.0	279.8	96.5	1.8	283.4	287.8	0.10
HT-0	10	252.0	280.8	91.6	2.8	282.2	289.5	7.40
HT-1	10	227.7	278.2	96.8	1.7	284.1	288.8	1.50
HT-2	10	248.0	279.3	95.5	1.8	283.6	288.3	0.40
HT-3	10	239.9	279.3	93.5	2.0	284.8	288.3	2.70
HT-4	10	242.2	279.3	96.4	1.8	283.9	288.7	0.18
HT-5	10	248.5	280.3	98.9	2.4	284.8	288.5	0.05
HT-7	10	151.1	274.7	84.0	1.0	280.5	284.6	11.90

Notes: β, heating rate, in °C min^{-1}; T_{ot}, onset temperature of decomposition; T_{oe}, onset temperature of the end decomposition; T_i , the initial temperature for thermal decomposition; T_p, the peak temperature of mass loss rate; Mass loss, from initial temperature to the end temperature of DTG peak, in wt.%; L_{max}, the maximum mass loss rate, in $\%.min^{-1}$.

Table S13. The non-isothermal DSC data of different HMX crystals doped with TAGP material.

		Endothermic peaks				Exothermic peaks			
Samples	β	T_i/ °C	T_p	T_e	ΔH_1	T_o	T_p	T_e	ΔH_2
HMX	10	192.1	199.5	206.4	-26.6	279.9	286.1	292.6	1574.1
HT-0	10	183.4	190.0	197.7	-24.7	279.5	288.9	291.2	1676.6
HT-1	10	-	-	-	-	278.3	286.4	291.0	1596.8
HT-2	10	-	-	-	-	278.9	286.9	292.1	1688.0
HT-3	10	177.2	187.1	199.0	-14.0	278.8	287.1	291.4	1684.8
HT-4	10	-	-	-	-	279.1	287.4	292.1	1610.0
HT-5	10	191.0	198.0	206.4	-27.9	279.4	287.5	292.0	1804.2
HT-7	10	-	-	-	-	278.2	282.8	290.1	804.0

Notes: β, heating rate, in °C min^{-1}; T_i , the initial temperature, in °C; T_o, onset temperature of the peaks, in °C; T_p, peak temperature of thermal events, in °C; T_e , the end temperature for heat change, in °C; ΔH_1, heat absorption, in $J.g^{-1}$; ΔH_2, heat release, in $J.g^{-1}$.

Table S14. The comparison for performances of the industrial β-HMX with CL-20 and the doped HMX.

Sample	Density	Formula	ΔH_c / J g^{-1}	ΔH_f / kJ mol^{-1}	VoD / m s^{-1}	P(C-J) /GPa	I_{sp}/ s	I_m/ J
β-HMX	1.886	$C_4H_{7.35}O_{8.44}N_{7.99}$	9634	283.30	9277/9158[e]	39.87	280.9	4.1
HT-0	1.620	$C_4H_{7.26}O_{8.44}N_{7.90}$	9667	283.31	8342	29.38	281.2	4.6
HT-1	1.869	$C_4H_{7.20}O_{8.43}N_{7.90}$	9659	289.73	9211	39.34	281.5	21.9
HT-4	2.040	$C_4H_{7.29}O_{8.39}N_{7.87}$	9709	280.23	9875/9292[e]	47.51	281.0	5.9
HT-7	2.131	$C_4H_{7.24}O_{8.41}N_{7.88}$	10362	487.38	10401	53.87	292.0	5.2
ε-CL-20	2.044	$C_6H_6O_{12}N_{12}$	-	377.04	9774	44.98	271.2	4.2

Note: superscript e means measured value using the same experimental setup.

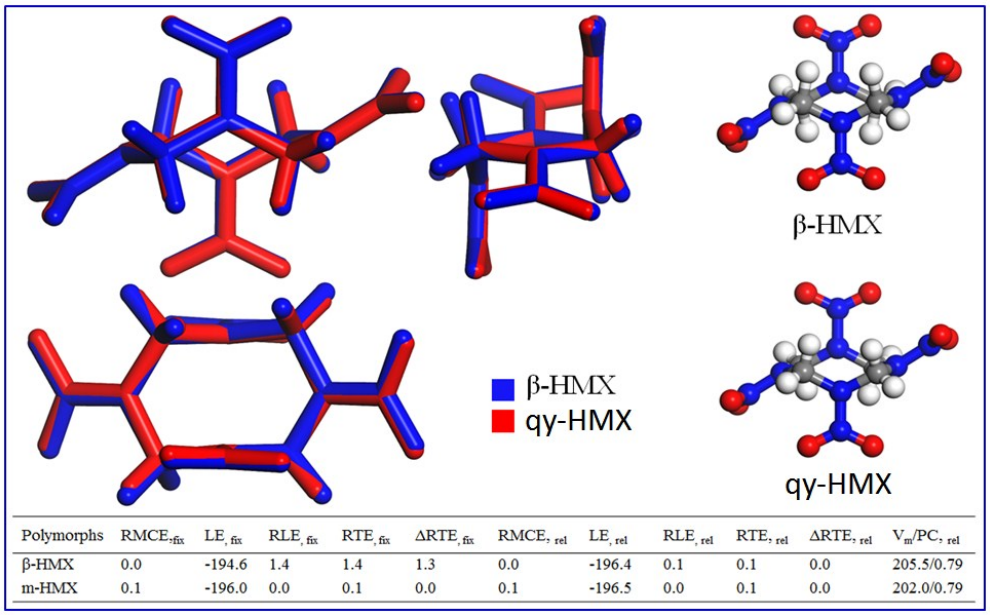

Polymorphs	$RMCE_{,fix}$	$LE_{,fix}$	$RLE_{,fix}$	$RTE_{,fix}$	$\Delta RTE_{,fix}$	$RMCE_{,rel}$	$LE_{,rel}$	$RLE_{,rel}$	$RTE_{,rel}$	$\Delta RTE_{,rel}$	$V_m/PC_{,rel}$
β-HMX	0.0	-194.6	1.4	1.4	1.3	0.0	-196.4	0.1	0.1	0.0	205.5/0.79
m-HMX	0.1	-196.0	0.0	0.1	0.0	0.1	-196.5	0.0	0.1	0.0	202.0/0.79

Figure S16. A comparison of the HMX molecule after compressing with permanent conformation change (qy-HMX) with conventional normal HMX molecule: a) The total energy of β-HMX is 1.3 kJ/mol, higher than that of m-HMX under the optimum condition, which indicates that qy-HMX is more stable than that of β-HMX; b) the difference of molecular conformational energy between the two types of HMX is only 0.1 kJ/mol, and the lattice energy of β-HMX is 1.4 kJ/mol higher than that of m-HMX. It shows that the conformation of HMX molecules has been slightly changed, and the difference in energy is large, and it reflects the varied packing arrangement of molecules in the cells.

Figure S17. Modeling powder of HT-4 and corresponding cylindrical pressed charges for detonation velocity measurements: the scaled-up HT-4 has an average density of 1.94 g cm^{-3}, but the pressed density is only 94% of the theoretical maximum density due to inhomogeneity of the crystals after scaling up.

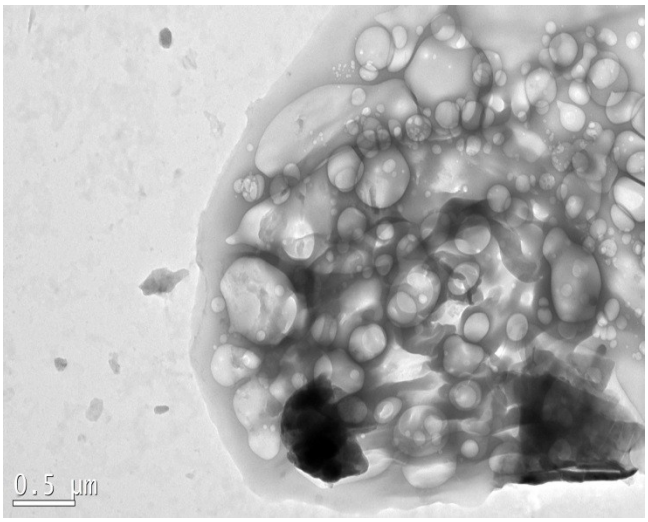

Figure S18. TEM image of dopant of qy-HMX after dissolving and filtration some block of tiny HMX crystals are still trapped inside the layers of TAGP.

References

[S1] Dolomanov, O.V., Bourhis, L.J., Gildea, R.J, Howard, J.A.K. & Puschmann, H. (2009), *J. Appl. Cryst.* 42, 339-341.

[S2] Sheldrick, G.M.. Acta Cryst. A71, 3-8 (2015).

[S3] Sheldrick, G.M.. *Acta Cryst.* C71, 3-8 (2015).

[S4] Cantrell J., Sullenger D., Miami University, Oxford, ohio, USA, ICDD grant-in-aid (1991); Sullenger D.,Cantrell J., Beiter T., *Powder Diffr*. 9, 2 (1994).

[S5] Choi C S, Boutin H P. A study of the crystal structure of β-Cyclotetramethylene Tetranitramine by Neutron Diffraction. *Acta Crystallogr B,* 26: 1235–1240 (1970).

[S6] M Herrmann, W Engel, N Eisenreich, Thermal expansion, transitions, sensitivities and burning rates of HMX, *Propell. Explos. Pyrot.,* 17, 190-195 (1992).

[S7] Rylance, J., Stubley, D. Heat capacities and phase transitions of octahydro- 1,3,5,7-tetranitro-1,3,5,7-tetrazocine (HMX), *Thermochim Acta*, 13 (3), 253-259 (1975).

[S8] W Lukasavage, S Nicolich, J Alster, Process of making impact insensitive Alpha-HMX, - US Patent 5,268,469, 1993.